AN INVESTIGATION OF METASTABLE ELECTRONIC STATES IN AB-INITIO SIMULATIONS OF MIXED ACTINIDE CERAMIC OXIDE FUELS

A Thesis
Presented to
The Academic Faculty

By

Adam Lord

In Partial Fulfillment
Of the Requirements for the Degree
Master of Science in Nuclear Engineering

Georgia Institute of Technology
December 2012

AN INVESTIGATION OF METASTABLE ELECTRONIC STATES IN AB-INITIO
SIMULATIONS OF MIXED ACTINIDE CERAMIC OXIDE FUELS

Approved by:

Dr. Chaitanya Deo, Advisor
NRE/MP Programs
George W. Woodruff School of Mechanical
Engineering
Georgia Institute of Technology

Dr. Farzad Rahnema
NRE/MP Programs
George W. Woodruff School of Mechanical
Engineering
Georgia Institute of Technology

Dr. Bojan Petrovic
NRE/MP Programs
George W. Woodruff School of Mechanical
Engineering
Georgia Institute of Technology

Date Approved: May 29, 2012

For my mother, who takes so much joy in even hearing the alien words which describe what I do, and is always eager for me to make another attempt to explain it to her.

For my father, who is a constant reminder to me that there is far more to good engineering than can be found in books and papers. Or theses.

ACKNOWLEDGEMENTS

TABLE OF CONTENTS

LIST OF TABLES

LIST OF FIGURES

SUMMARY

First-principles calculations such as density functional theory (DFT) employ numerical

approaches to solve the Schrodinger equation of a system. Standard functionals employed

to determine the cohesive system energy, specifically the local density and generalized

gradient approximations (LDA and GGA), underestimate the correlation of $5f$ electrons to

their ions in AO_2 systems (A=U/Pu/Np). The standard correction, the "Hubbard +U,"

causes the multidimensional energy surface to develop a large number of local minima

which do not correspond to the ground state (global minimum). Because all useful energy

values derived from DFT calculations depend on small differences between relatively

large cohesive energies, comparing systems wherein one or more of the samples are not

in the ground state has the potential to introduce large errors.

This work presents an analysis of the fundamental issues of metastable states in both pure

(e.g. UO_2) and binary (e.g. $U_{0.5}Pu_{0.5}O_2$) AO_2 systems, investigates novel methods of

handling them, and describes why current literature approaches which appear to work

well for the pure compounds are not well-suited for systems containing multiple actinide

species.

CHAPTER 1: INTRODUCTION

1.1 Overview of Work

A theoretical background regarding first-principles calculations, in particular density functional theory, is given. The incomplete description of highly-correlated systems such as actinide oxides is explained, as is the problem of metastable states, the fundamental disadvantage to the Hubbard +U correction, the prominent current solution employed for such systems. A literature review is presented, outlining existing work done concerning the modeling of nuclear ceramic oxide (AO_2, A=U, Pu, and/or Np) fuels. The use of a volume-energy curve is proposed as not only as a tool to derive a material's elastic properties, but also as a litmus test for the effectiveness of any attempted approach in solving the issue of metastable states. Current literature approaches to the metastable issue for pure actinide oxides (i.e. UO_2, PuO_2, and NpO_2) are described, and simpler solutions are presented and tested using the volume-energy curve approach. The methods introduced are then shown to fail for systems containing multiple actinide species (e.g. $U_{0.25}Pu_{0.75}O_2$), and problems with the existing methods to approach such systems are discussed.

1.2 Motivation

Uranium dioxide, UO_2, is the predominant fuel component in modern nuclear power reactors[1]. The presence of transuranics in spent fuel, most notably plutonium, neptunium, americium and curium, represent both proliferation and storage concerns. An alternative to on-site storage or repository disposal is the recycling of these "waste" products and

inserting them into the fuel cycle for the purposes of breeding or transmutation[2]. In MOX fuel, some fraction of the uranium in the crystal matrix is replaced by plutonium and/or other minor actinides. Even in pure urania, by far the most extensively-studied of the actinide oxides, the driving mechanisms behind phenomena such as oxygen diffusion and fission product/gas retention remain poorly understood. To this end, multi-scale modeling can be a powerful tool.

Computational materials simulations can be performed at many scales of time and length resolution, as illustrated in Figure 1, and can be used effectively in combination with one another. A kinetic Monte Carlo (kMC) simulation investigating oxygen diffusivity may set its defect concentrations based on a molecular dynamics (MD) result, while the parameters for the semi empirical inter-atomic potentials used in the MD simulation are heavily based on energies calculated from first principles.
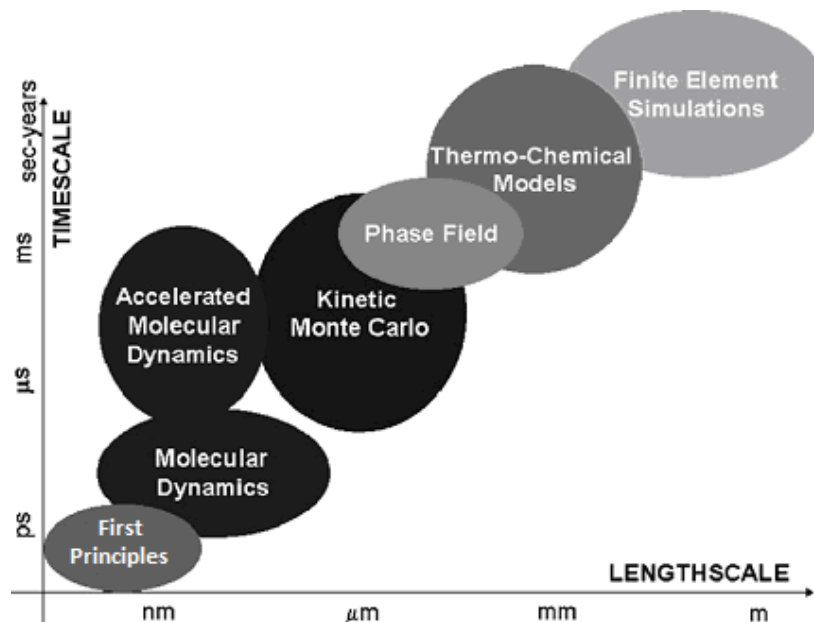
Figure 1: Time and length scales of modeling and simulation of materials[3]

At the smallest length scales and shortest time scales, quantum mechanical effects can be treated directly. This high-resolution approach to modeling systems is referred to as "first-principles" or "ab-initio," and calculates a system's electronic wavefunction $\psi(\bar{r})$ explicitly. A first principles simulation calculates the total energy of the system, though in all practical applications, it is not this total energy but rather the energy differences between similar systems which are most important. When implemented effectively, the energy differences can be used to derive formation energies of defects, migration energies, and even certain bulk properties such as the equilibrium lattice constant (and, thereby, the density) or the bulk modulus.

1.3 Actinide Dioxides

Urania, plutonia, and neptunia are chemically very similar. Each is a fluorite-structured ceramic[1] with a melting point exceeding 2400°C, well above operating temperatures found in any nuclear reactor.
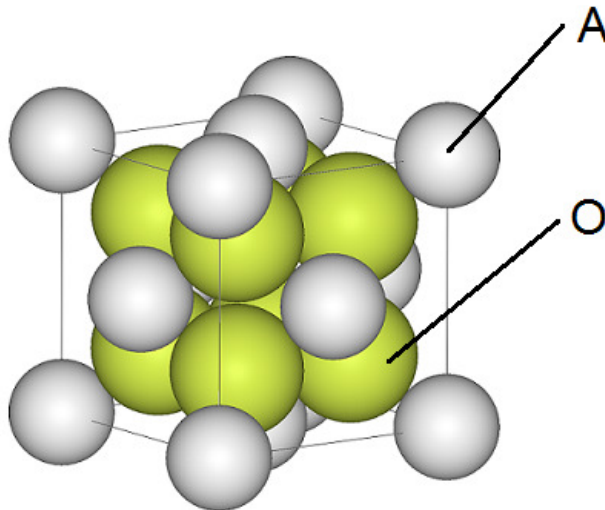
Figure 2: The fluorite structure of AO_2

The fluorite structure represents the actinides on an oversized FCC lattice, with eight oxygen ions per unit cell located at the tetrahedral holes, effectively forming a simple cubic sublattice. Table 1 lists the experimentally measured lattice parameter and bulk modulus of each actinide oxide at room temperature.

Table 1: Bulk Properties of Actinide Oxides

	a_0 (Å)	B_0 (GPa)
UO_2	5.47[4]	207[5]
PuO_2	5.398[6]	178[5]
NpO_2	5.43[4]	200[5]

At temperatures below 200 K, a Jahn-Teller effect is observed in urania, displacing the oxygen sublattice from its idealized location by 0.014 Å in the <1 1 1> directions[7]. At temperatures below 30.8 K, AFM ordering causes the unit cell to deform from cubic to tetragonal[8], with $a_0 \approx 1.01 c_0$.

CHAPTER 2: THEORY AND LITERATURE REVIEW

2.1 Overview of Density Functional Theory

Density Functional Theory (DFT) is so named for the modeling of "smeared" electronic wavefunctions as a gas. The density of this gas varies proportionally with the magnitude of the system's electronic wavefunction. For a given geometric configuration of ions, a first-guess of the system's wavefunction is generated by randomly generating a wavefunction for each of its N electrons. The individual wavefunctions $\Psi_i(\vec{r})$ yield an effective charge distribution $V_{ext}(\vec{r})$ defined by

$$V_{ext}(\vec{r}) = \sum_{i=1}^{N}\left(\frac{1}{4\pi\varepsilon_0}\cdot\int\frac{n_i(\vec{r}')}{|\vec{r}-\vec{r}'|}d^3\vec{r}'\right) \tag{1}$$

Where

$$n_i(\vec{r}') = |\psi_i(\vec{r}')|^2 \tag{2}$$

represents the effective probability that an electron with the wavefunction $\psi_i(\vec{r}')$ will be found at location $\vec{r}'$, and ε_0 is the permittivity of free space. Because the *N*-electron problem may be formally rewritten as an exactly equivalent set of *N* one-electron equations[9], the wavefunction for each electron is now solved for directly via the Schrodinger equation.

$$\frac{-\hbar^2}{2m}\nabla^2\psi_i(\vec{r})+V_{ext,i}(\vec{r})\psi_i(\vec{r})=E\psi_i(\vec{r}) \tag{3}$$

The external potential is slightly modified, to include Coulomb effects from the system's ions, treated as simple point charges, and to remove the electron's own contribution from the potential.

$$V_{ext,i}(\vec{r}) = \sum_{j \neq i}^{N} \left(\frac{1}{4\pi\varepsilon_0} \cdot \int \frac{n_j(\vec{r}')}{|\vec{r} - \vec{r}'|} d^3\vec{r}' \right) + V_{ion}(\vec{r})$$ (4)

$$V_{ion}(\vec{r}) = -\sum_{k=1}^{M} \frac{1}{4\pi\varepsilon_0} \cdot \frac{Z_k e}{|\vec{r} - \vec{R}_k|}$$ (4a)

Z_k and $\vec{R}_k$ denote the atomic number and position of the kth ion. The system's energy eigenvalue E is calculated (see Section 2.3), and the electron's wavefunction is determined. Once all electrons have been treated, the process of generating an external potential and solving the individual wavefunctions can be iterated until the wavefunctions have sufficiently converged. This is known as the "self-consistent" condition, referring to the physical implication that the converged spatial distribution of charges gives rise to an electrostatic potential which, if imposed artificially, would require a system populated by those charged particles to have that same spatial distribution. In practice, the ions are held in fixed geometric positions per the Born-Oppenheimer approximation (BOA) until the electronic wavefunctions have been converged. The ions are then allowed to relax according to any of multiple methods, and the electrons are again converged, using their most recent wavefunctions to initialize. The final system energy is calculated after each geometric relaxation step, and is given its own convergence criterion.

2.2 The Form of the Energy Functional

The system's wavefunction alone is sufficient to uniquely determine its cohesive energy, provided the electronic component is treated as a uniform electron gas with spatially varying density $n(\vec{r})$. It is also the case that the density of the electron gas at any point is simply equal to the sum of the probabilities of finding each individual electron at that point. That is, from equation 2,

$$n(\vec{r}) = \sum_{i=1}^{N} n_i(\vec{r}) \tag{5}$$

Hohenberg and Kohn[10] proved the existence of a universal functional $E[n(\vec{r})]$, which has as its global minimum the ground-state energy of the system. The form of the functional and, more importantly, tractable approximations to it, have been the subject of extensive research. Kohn and Sham[11] expressed the functional as a simple summation of particle type interactions—electron/electron, ion/electron, and ion/ion—as well as the kinetic energies and exchange-correlation effect. The correlation energy arises from the fact that the energy limit of the iterative approach lies above the exact energy, and is a product of simplifying assumptions such as BOA[12]; the exchange energy is a quantum effect, and effectively increases repulsion between identical particles such as fermions (e.g. electrons)[13].

With the electrons' wavefunctions determined and the ions' motion neglected, the kinetic energy of the system is simply a summation of the individual electrons' kinetic energies.

$$KE = 2\sum_i \int \psi_i \left[-\frac{\hbar^2}{2m} \right] \nabla^2 \psi_i d^3\vec{r} \tag{6}$$

The ion-ion repulsion, arising from *M* point charges, must be treated by counting each interaction explicitly, excluding self-interactions and correcting for double counting.

$$PE_{ion-ion} = \frac{1}{2} \sum_{k=1}^{M} \left(\sum_{k' \neq k} \frac{(Z_k e)(Z_{k'} e)}{\left| \vec{R}_k - \vec{R}_{k'} \right|} \right) \tag{7}$$

The ion-electron potential energy is treated sweepingly, using the total electron density from equation 5 and the total effective ionic potential from equation 4a.

$$PE_{ion-electron} = \int V_{ion}(\vec{r}) n(\vec{r}) d^3\vec{r} \tag{8}$$

Likewise, the electron-electron component is simply

$$PE_{electron-electron} = \frac{e^2}{2} \int \frac{n(\vec{r}) n(\vec{r}')}{\left| \vec{r} - \vec{r}' \right|} d^3\vec{r} d^3\vec{r}' \tag{9}$$

The only component not directly calculable from wavefunctions is the exchange-correlation functional $E_{XC}[n(\vec{r})]$. Although a multitude of approaches and specific models exist, the two most successful methods found in actinide-focused literature are also the simplest. They are briefly discussed in the following two subsections.

2.2.1 Local Density Approximation (LDA)

Kohn and Sham also proposed an approximate form for the exchange-correlation functional, based solely on the local value of the electron gas density multiplied by an exchange-correlation function $\varepsilon_{XC}(n)$.

$$E_{XC,LDA}[n(\vec{r})] = \int \varepsilon_{XC}(n(\vec{r})) \cdot n(\vec{r}) d^3\vec{r} \qquad (10)$$

Early forms of $\varepsilon_{XC}(n)$ focused on the Dirac-Gasper-Kohn-Sham potential[11]

$$\varepsilon_{XC}(n) \equiv \mu^x(\vec{r}) = -\frac{e^2}{\pi} \cdot \sqrt[3]{3\pi^2 n(\vec{r})} \qquad (11)$$

Slater[14] proposed scaling this by a constant factor α, and Gunnarsson and Lundqvist[15] further refined it by replacing α with a semiempirically fitted scaling factor β(n). The startling success of such a simple approximation has been found to at least partially arise from a fortunate offsetting of errors: an overestimation of the exchange energy, and an underestimation of the correlation energy[16].

2.2.2 The Generalized Gradient Approximation

If the LDA is considered a "zeroth order" approximation, then the generalized gradient approximation (GGA) can be said to include first-order expansion terms. The exchange-correlation functional here has the form

$$E_{XC,GGA}[n(\vec{r})] = \int \varepsilon_{XC}(n, \nabla n) \cdot n(\vec{r}) d^3\vec{r} \qquad (12)$$

A GGA functional may be developed ab-initio, or through empirical parameterization, being fitted to a reference set[16]. Any work described in this thesis which employs a GGA functional has always used the PBE instantiation of the method, in which all parameters involved are derived from first-principals constraints[17]. Other unfitted functionals include BLYP[18] and PKZB[19], with the latter incorporating some semi-local properties. In general, GGA surpasses LDA in calculations of absolute binding energies, but not in calculations of structural properties such as the equilibrium lattice constant, which is determined by

comparing energy differences as opposed to absolute energies. There is no systemic GGA

advantage in the calculation of bulk properties, though select formalisms such as PBE

definitively surpass established LDA methods over a broad range of crystals and

molecules[16].

LDA and GGA may each be modified to include a term accounting for spin interactions.

However, prior publications have shown that spin corrections do not appreciably affect

bulk properties of either UO_2[20] or PuO_2[21]. Some of the original work to be presented here

employs the spin correction, but those portions are isolated and the general conclusions

drawn do not depend on use of the spin correction.

2.3 Periodicity and Supercells

Including a sufficiently large number of ions within an isolated system to model a bulk

crystal is computationally intractable within DFT. And while reducing an *N*-electron

system to a set of *N* noninteracting one-electron systems is trivial, defining a periodic

crystalline system effectively yields an infinite number of electrons interacting with one

another, as well as with an infinite number of ions. Because the system also extends

infinitely into space, each wavefunction would also require expansion in an infinite

number of plane waves. Unlike the fundamental intractability of a large isolated system,

however, each of these computational roadblocks in periodic systems has a well-

established method suited to overcome it.

2.3.1 Bloch's Theorem

Bloch's theorem addresses the issue of infinite spatial expansion, noting that the wavefunction of each electron may be rewritten as a periodic component, needing definition on only the domain of the unit cell, and a wavelike component[22].

$$\psi_i(\vec{r}) = f_i(\vec{r}) \exp(i\vec{k} \cdot \vec{r}) \tag{13}$$

The now-finite periodic component can now be expanded using standard techniques, choosing the basis set to have its wave vectors $\vec{G}$ defined as the reciprocals of the unit cell's lattice vectors $\vec{l}_a$, $\vec{l}_b$, and $\vec{l}_c$. That is,

$$f_i(\vec{r}) = \sum_G a_{i,\vec{G}} \exp(i\vec{G} \cdot \vec{r}) \tag{14}$$

Where $\vec{G} \cdot \vec{l}_q = 2\pi m$, and m is an integer. The rewritten wavefunctions now have the form

$$\psi_i(\vec{r}) = \sum_G a_{i,\vec{k}+\vec{G}} \exp\left[i(\vec{k}+\vec{G}) \cdot \vec{r}\right] \tag{15}$$

The Bloch theorem transforms the problem of calculating an infinite number of electrons' wavefunctions into one requiring calculation of a finite number of wavefunctions, albeit each wavefunction requiring evaluation at an infinite number of k-points, each k-point encompassing an infinite number of basis plane waves.

2.3.2 Selection of Sample k-points

The k-points populate the Brillouin zone, effectively defined as the periodic cell in reciprocal space. Since the wavefunctions represented by nearby k-points are very

similar, results of high accuracy may be obtained with tractable computational effort by choosing an appropriate subset of k-points, an acceptable granulation of reality not unlike approximating the area under a curve as a series of rectangles. The problem has therefore been reduced to a finite number of wavefunctions, each evaluated at a finite number of k-points, leaving only the infinite number of basis plane waves to be addressed. The algorithm used to select k-points for this work was developed by Monkhorst and Pack[23].

2.3.3 Cutoff Energy

The magnitudes of the coefficients $a_{i,\vec{k}+\vec{G}}$ in equation 15 diminish rapidly with increasing kinetic energy (given by $\left(\hbar^2/2m\right)\cdot\left|\vec{k}+\vec{G}\right|^2$). The periodic component, then, need only be expanded in basis waves representing kinetic energies below some ceiling, or "cutoff," energy.

Convergence tests must be run for any application, to determine the k-point mesh density and cutoff energy necessary for convergence. The loss of precision caused by a coarsened k-point mesh should be negligible compared to any energy values or differences which are being investigated. Choices found in representative publications investigating actinide compounds include mesh densities ranging from 4x4x4 to 8x8x8, and cutoff energies ranging from 400-900 eV[24,25,26,27,28,29]. This work uses a 4x4x4 k-point mesh and a cutoff energy of 700 eV (see Subsection 4.1.2).

2.3.4 Supercells

In many DFT applications, it is the formation or migration energy of a defect which is being investigated. Because a defect-containing periodic system consisting of only a

single unit cell would force the defect to interact with its own "mirrors," a larger system is often used, such as a 2x2x2 system of 8 unit cells, which drastically reduces the magnitude of self-interaction. This is only due to the isolated nature of defects; in a pure bulk system, a 1x1x1 cell is sufficient.

2.4 Pseudopotential Approximations

Interactions between atoms depend much more strongly on valence electrons than on core shell electrons. This fact can be exploited to drastically reduce the computational demand of the simulation. The all-electron wavefunction oscillates rapidly near the atomic nucleus, and a very high cutoff energy is needed to follow its variation. If the critical properties of the all-electron potential are replicated with a more slowly-varying pseudopotential, a much lower cutoff energy can suffice.

Figure 3 shows an example of such a pseudopotential, and the electrostatic potential it effects. Past some "core" radius r_c, the pseudopotential matches the all-electron potential exactly. Within the core radius, its behavior is chosen such that specific properties of the all-electron potential are replicated; scattering properties, phase shifts, and norm conservation (preservation of total core charge) are universal targets. The pseudopotential in Figure 3 is nodeless, a desirable feature when seeking a function easily expandable in low-energy eigenfunctions[9].
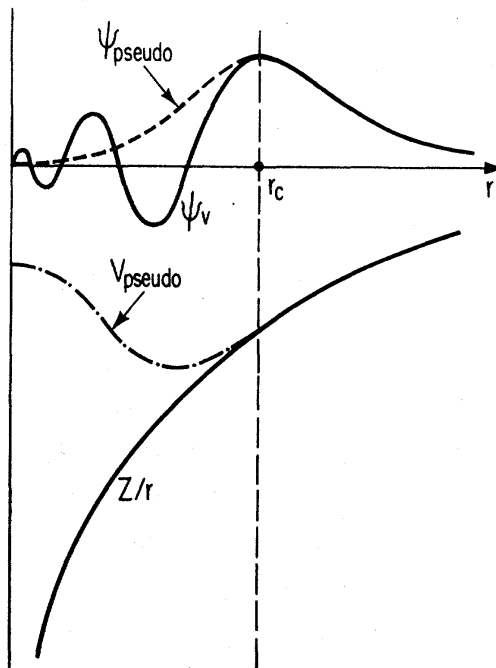
Figure 3: A pseudopotential compared to the all-electron potential

For a more technical discussion of pseudopotential theory and construction, see "Theory of Pseudopotentials" by David Vanderbilt, and [9].

2.5 Hubbard +U Correction and the Origin of Metastable States

Despite the general success of LDA and GGA, actinide oxides are a well-documented example of their shortcomings. In particular, both functionals drastically underestimate the correlation of the $5f$ electrons to their host actinide ion, modeling those electrons as highly delocalized[30]; in UO_2, $5f$ electrons behave as if the system were pure metallic α-uranium. In reality, those electrons are strongly correlated to one specific uranium ion, and the system is not a metallic conductor but an insulator with a bandgap of 1.3 eV[31]. The delocalization manifests itself as an abundance of partial atomic orbital occupancies in the ground state; the degree of occupation of an orbital is calculated by taking the inner

14

product of the electron's wavefunction and the given orbital. As shown in a very conceptual sketch in Figure 4, the global energy minimum lies at a state involving a non-integral occupation of the atomic orbital denoted on the horizontal axis.
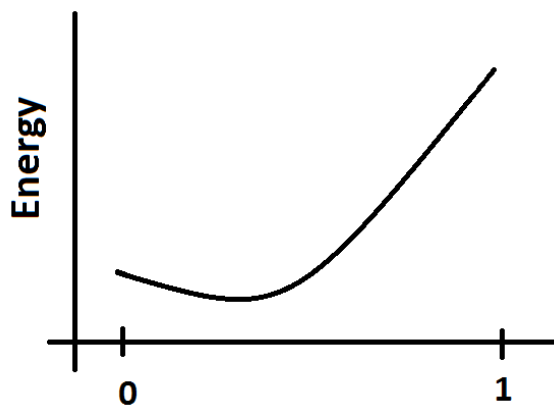
Figure 4: Global energy minimum at a partial occupancy of an atomic orbital
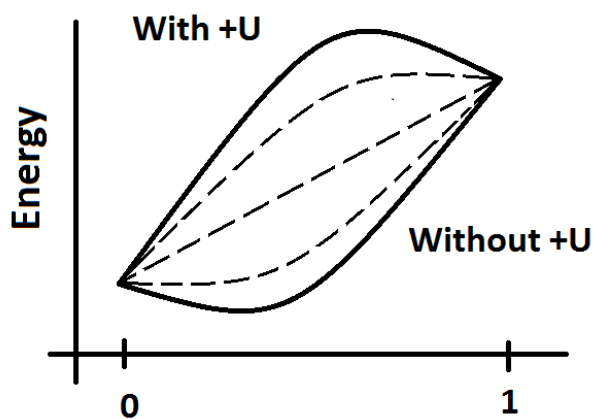
Figure 5: Multiple local energy minima at integral orbital occupations

To address this issue, seen in both LDA and GGA, the Hubbard approach[32] effectively imposes an energy penalty on electrons which attempt to partially occupy an atomic orbital. This energy penalty, imposed to a sufficient degree, requires valence electrons to

integrally occupy states which more closely resemble the atomic orbitals of their native ion[33]. The modified energy surface now conceptually resembles the sketch in Figure 5. After the +U modification has been implemented, the energy surface becomes convex, and develops local minima.

Local minima which are not also the global minimum are referred to as "metastable states" because the energy minimization scheme will converge to their location under certain initial guesses, but they are not the ground state. Because all predictions of physical properties by DFT are dependent on the relatively small energy differences between systems, comparing one system's ground state to another system's metastable state can dramatically skew the results.
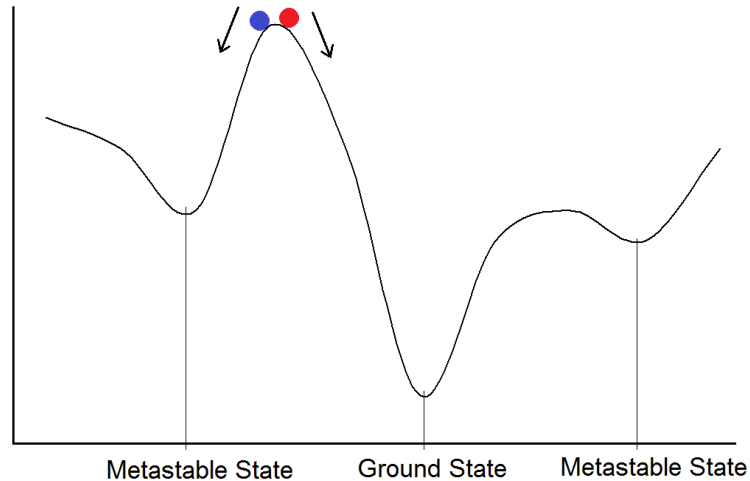
Figure 6: Effects of the initial guess on the final converged state

Figure 6 illustrates the sensitivity of the converged state to the initial conditions. A DFT simulation probes not simply a one-dimensional energy curve but a highly dimensional energy surface; the initial conditions include not only the electronic wavefunctions but

the volume of the system and the positions of the ions. UO_2 is a cubic fluorite structure

(high symmetry) at room and reactor temperatures, but at the 0 K conditions present in

DFT calculations, both the Jahn-Teller distortion of the oxygen sublattice and the unit

cell transformation to tetragonal act to subvert this symmetry.

2.6 Current Approaches to Metastability

Understanding and avoiding the metastable states created by the necessary +U correction

is a central issue in any DFT study of actinide dioxides. Successful approaches have been

published for pure UO_2 by Dorado[30] and Meredig[33]. Neither approach has been extended

to pure PuO_2 or NpO_2, or to any mixed oxide (MOX) systems. In fact, to date no

literature has taken a close look at bulk MOX systems at all from a DFT perspective.

2.6.1 Electronic Orbital Control (EOC)

Dorado's method amounts to a combinatorial search of initial conditions to uncover the

ground state through brute force. A computational protocol is established, requiring the $5f$

electrons to occupy particular atomic orbitals during the first 10 electronic iterations

before any geometry relaxation is allowed. Subsequently, the controls are released and

the simulation converges with no further restrictions. After running a series of $_7C_2 = 21$

simulations imposing various orbital restrictions (valence electrons occupying two of

seven $5f$ orbitals), the lowest energy observed was reached by four of the simulations,

each showing the same final occupation matrix. It was put forth that this occupation

matrix could be imposed at the outset of the calculation, and if the same occupation

existed after final convergence, the results must represent the ground state.

2.6.2 Hubbard Parameter Ramping

The approach by Meredig seeks to exploit the qualitative nature of the energy surface. As was shown in Figure 4, the presence of the Hubbard correction has introduced convexities. The convexity is amplified for larger Hubbard parameters, and for sufficiently small values the surface remains concave at all points. Intermediate values are represented by the multiple dashed curves.

The results of a DFT simulation include the system's converged electronic wavefunctions, charge densities, and ion positions. In the Meredig protocols, a first simulation is run with no Hubbard correction. The three output files listed are then used to initialize a second simulation which is identical to the first save for the introduction of the Hubbard +U parameter, at a small fraction of its actual value. If the established value of U_{eff} is 4 eV, this second run may use 0.25 eV or 0.50 eV. The energy surface is slightly less concave, and the fractional orbital occupation converges to an intermediate value between the lowest-energy states indicated by Figures 4 and 5. The process is iterated, incrementing U_{eff} to its full value with the expectation that the fractional orbital occupation will gradually "slide" to the lowest-energy integral occupation for the final simulation. It should be stressed that these figures are qualitative, and the ground state of DFT+U simulations found by Dorado does not show integrally occupied orbitals.

The ramping scheme was tested against the EOC combinatorial search for a 1x1x1 UO_2 system, and its proposed ground state lay roughly 0.06 eV above that found by EOC's

enumeration. For another system, distorted CoO, it revealed a state lying below EOC's

prediction[33].

CHAPTER 3: THE VOLUME-ENERGY CURVE

As briefly mentioned in Section 1.2, DFT can be used to derive a prediction for the lattice constant of a system. More typically, the plot is unit cell volume, rather than lattice constant, versus energy. The concept is now illustrated in Figure 7. The energies are fitted to a known theoretical "equation of state," the fitting parameters of which are physical properties of the material such as the equilibrium unit cell volume V_0 (lattice constant $a_0=V_0^{1/3}$), the equilibrium cohesive energy E_0, and the bulk modulus B_0.
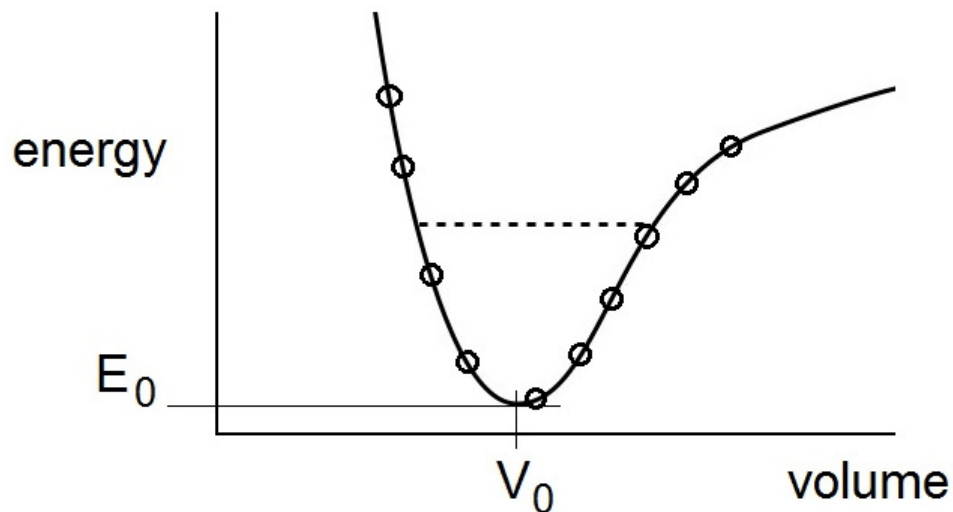
Figure 7: Generic volume-energy curve

The broad range of system volumes in Figure 7 is shown to illustrate the asymptotic behavior of the curve at small and large volumes; only a very narrow range of system sizes near the equilibrium need be computed to fit a reliable curve, representing a strain on the order of $\pm 1\%$. Such a deformation is unlikely to be exceeded in real solids, especially ceramics such as actinide dioxide fuels.

3.1 Equation of State

The equation of state chosen to fit the data done by this work is simplified one which assumes a constant bulk modulus B_0.

$$E = E_0 + B_0\left(V_0 - V + V \cdot \ln\left(V/V_0\right)\right) \qquad (16)$$

If we are careful to normalize our volumes to Å^3, we can separate the ratio within the logarithm to yield a three-parameter model which can be easily fit to a data set using multiple linear regression.

$$E = \left(E_0 + B_0 V_0\right) + B_0\left[V \cdot \ln(V)\right] + \left[B_0 \cdot \ln(V_0) + B_0\right] \cdot V \qquad (17a)$$

$$E = a + b \cdot \left[V \cdot \ln(V)\right] + c \cdot V \qquad (17b)$$

The fitted parameters are functions of the predicted properties V_0, B_0, and E_0, and can be solved for simultaneously with little effort. In this work, all data sets are normalized with respect to the lowest energy found in the set, and so any value of E_0 is relative to this point; in any case, it is not used in analysis.

Although more sophisticated models do exist, most notably those developed by Murnaghan[34] and Birch[35], the computational effort involved in fitting them to data does not yield a noticeable improvement over the volume ranges which are considered by this work. Using the experimentally known lattice parameter[4], bulk modulus[5], and variation in the bulk modulus due to stress[5] for UO_2, the three models are compared over relevant system volumes in Figure 8.
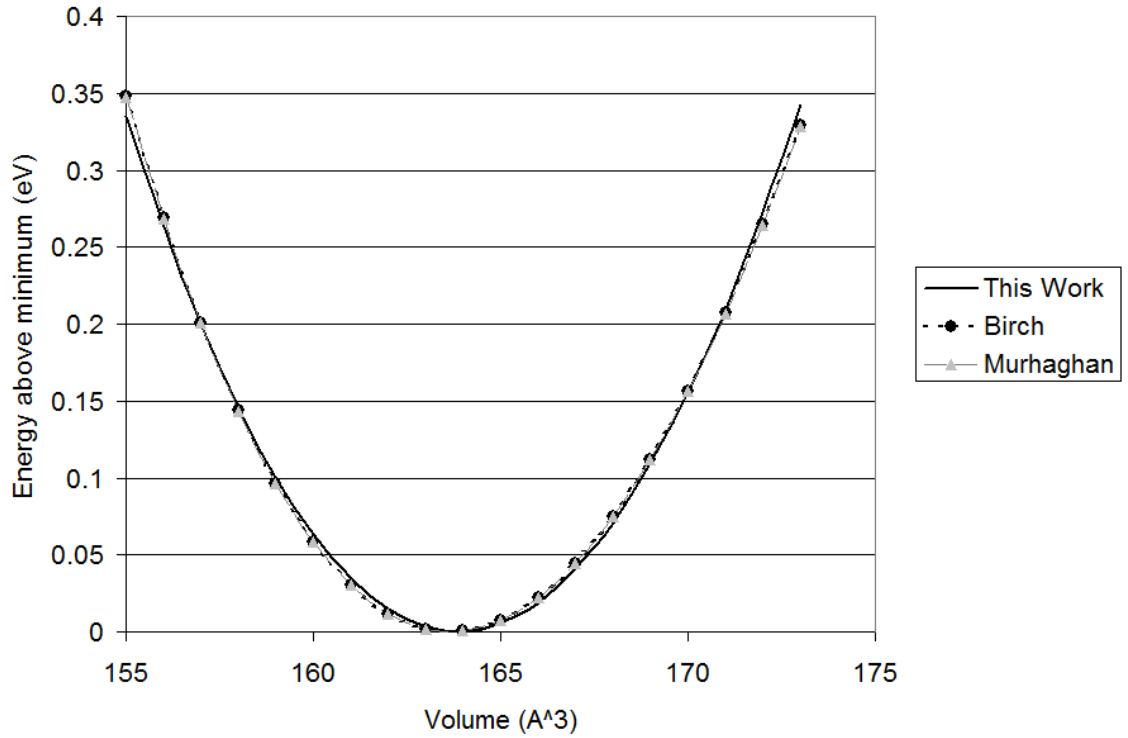
Figure 8: Comparison of Various Equations of State

Experimental information regarding stress-dependence of the bulk modulus is not available for PuO_2 or NpO_2, or for any mixed composition. Based on their similarities to UO_2, it is reasonable to assume the model used in this work is equally as valid for those oxides as well.

3.2 Using the Volume-Energy Curve to Detect Metastable States

Figure 9 is a volume-energy plot of eight simulations, with the systems' lattice constants ranging from 5.18 Å to 5.32 Å, incremented by 0.02 Å. Because total energies mean little, the results were normalized, treating the lowest energy as the zero point. The functional used was GGA-PBE, and did not employ the Hubbard +U correction, and so the energy surface was concave, devoid of potential metastable states. The equilibrium

values predicted by the curve are a_0=5.25 Å and B_0=221 GPa. This underestimation of

the lattice parameter is typical of actinide DFT calculations with no +U considerations.
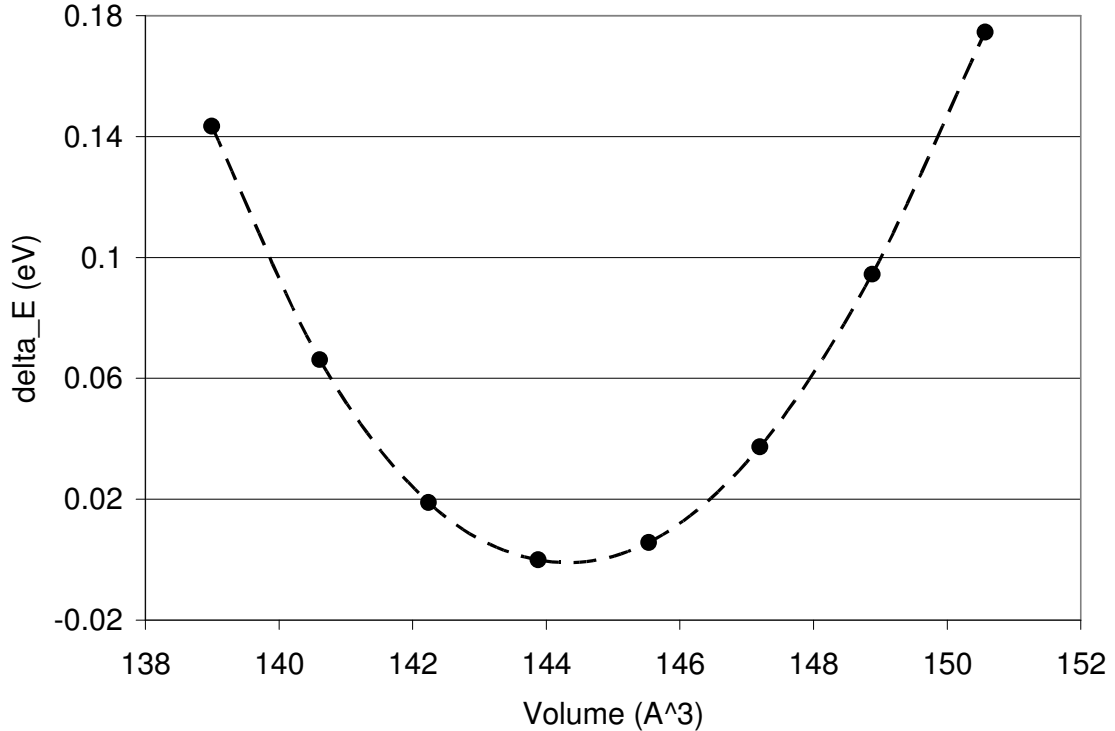
Figure 9: Sample volume-energy curve from $Pu_{0.5}Np_{0.5}O_2$ using GGA

Note the energy differences between consecutive system sizes are on the order of several

hundredths of an eV. This is small compared to other energy differences looked at in

literature—primarily defect formation and migration energies—which are on the order of

1-10 eV[1,8,27]. If there were any metastable states represented by these converged systems,

they would have to lie much less than 0.01 eV above their ground state, and would have a

negligible influence on DFT predictions. Using formation/migration energies themselves

as a proxy for ground states, however, carries risk. The method under investigation may

leave the systems in metastable states lying several tenths of an eV above their ground

states but result in an energy difference which is within the acceptable range of error. Because metastable states have been observed (though infrequently) which lie several eV above their ground state[30], such a method could pass a spot check and later give very wrong results. By vetting the method using a volume-energy curve, it is required to successfully converge to a ground state in every system, and if one or more systems become stuck in any metastable state, the deviation will be readily apparent. If a method can converge a system to any metastable state, even if that state lies not far above the true ground state, then it is likely susceptible to much larger deviations as well.

3.3 Magnitude of Metastable States

By running a series of systems similar to those in Figure 9 through a DFT+U functional, we can gain some insight into exactly how high above the ground state a metastable state can lie. Figure 10 shows the collective results of two sets of runs: one ranging from 5.1-5.7 Å in increments of 0.1 Å, and one much more densely spaced—from 5.35-5.45 Å in increments of 0.01 Å.

The energy differences between widely-spaced systems are on the order of several eV. The metastable states are clearly visible near the minimum of the curve, and are roughly one order of magnitude smaller. They may be present in the extreme system sizes, but are masked by the larger inherent energy differences. The energy differences between narrowly-spaced systems, from which the bulk properties must be derived, are an order of magnitude smaller still, and all information in this region of the curve is lost amidst metastable noise.
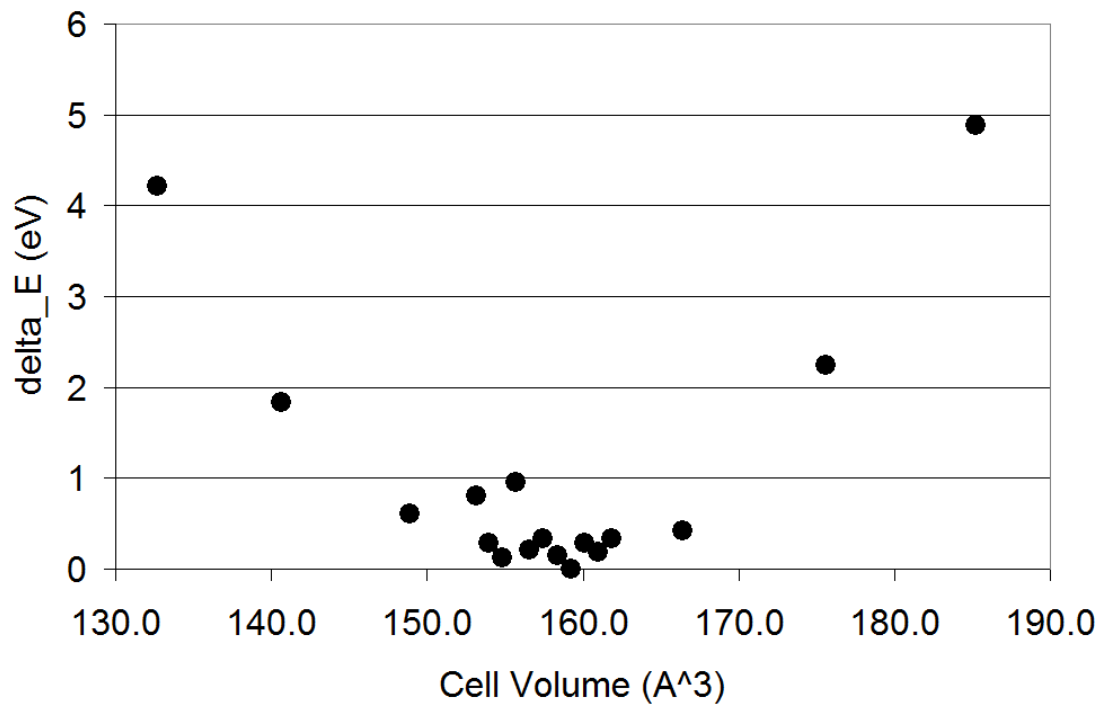
Figure 10: Finely and coarsely spaced system sizes for $U_{0.5}Pu_{0.5}O_2$

CHAPTER 4: METHODOLOGY AND APPROACHES TO METASTABILITY

4.1 Vienna Ab-initio Software Package (VASP)

4.1.1 General Parameters

All simulations were done using VASP[36,37]. System cell volume and shape were kept rigid, with one exception noted in Section 4.2. Ion positions were allowed to relax in all cases, and were typically initialized as ideal fluorite. Exceptions to this are limited to the distorted structure referenced in Figure 16, and all structures in Section 4.5 which took as their initial structure the final structure from a prior simulation. The unit cell chosen was a 1x1x1 12-atom supercell, containing 4 actinide ions and 8 oxygen ions.

4.1.2 Convergence Considerations and Determination of Parameters

The electronic convergence criterion was set to 0.1 meV. A cutoff energy of 700 eV was chosen. Convergence tests were run at this cutoff for various k-point mesh densities and compared with a computationally taxing "benchmark" simulation using hundreds of k-points. Results are shown in Figure 11. The 4x4x4 mesh showed a deviation of just over 1 meV per UO_2, or 0.05 eV per 12-atom unit cell. This is sufficient for ground state calculations. Applicable Hubbard parameters, listed in Table 2, were taken from Kotani and Yamazaki's experimental data[38]. The Dudarev[39] implementation of +U, which considers only the quantity U-J rather than their distinct values, was used for calculations.

Table 2: Choice of Hubbard Parameters

Element	U (eV)	J (eV)	$U_{eff} = U-J$ (eV)
U	4.5	0.51	3.99
Pu	4.0	0.75	3.25
Np	5.0	0.61	4.39
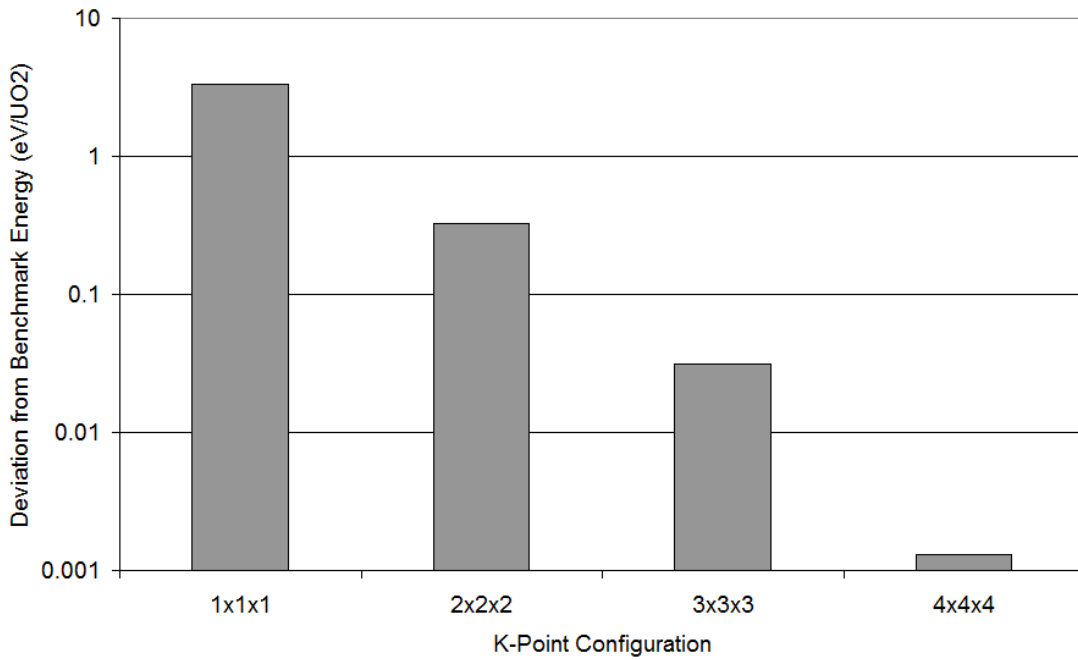
Figure 11: K-points convergence test

4.2 Ideality of the Solid Solutions

Because there is minimal experimental data regarding the lattice constants and bulk

moduli of mixed actinide oxides, it is necessary to estimate their values from the known

properties of the pure compositions. Published values are limited to lattice constants of

urania-plutonia[40] and urania-neptunia[4] systems, which were found to obey Vegard's law.

Vegard's law states that, for ideal solid solutions, the elastic properties and equilibrium lattice constant should vary linearly with composition for mixtures[41]. As chemically and physically similar compounds, the actinide dioxides are prime candidates to form solid solutions. A litmus test for a solid solution is the cohesive energy of the system; if it is linear with respect to composition, the solution is ideal.

The simulation parameters for this test were slightly different than the standard settings listed in Section 4.1. To achieve full relaxation, cell size and shape were allowed to change, in addition to the basic ion position relaxation. All binary MOX combinations were tested in a 1x1x1 system, and each pair returned results which strongly support the ideality of the solution. A sample of the data, the normalized energies of the U-Pu MOX systems, is included as Figure 12.
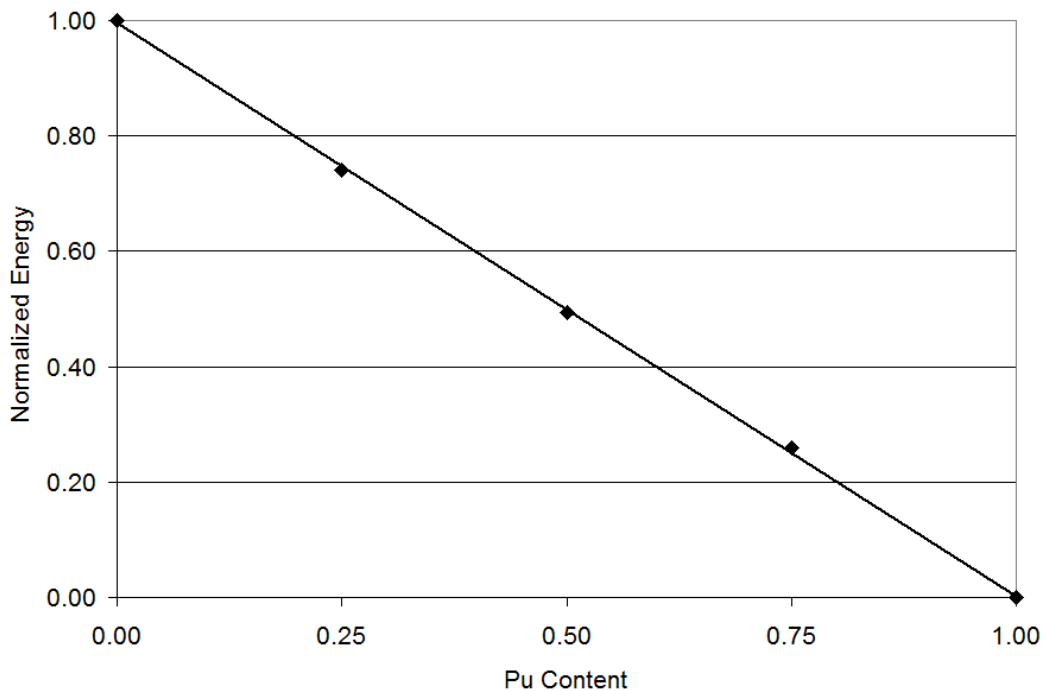
Figure 12: The ideality of $(U,Pu)O_2$

4.3 Establishing a Baseline Using Unmodified GGA

A full set of energy-volume curves was generated for pure UO_2, PuO_2, NpO_2, and for all binary combinations $A_xB_{1-x}O_2$, using the GGA-PBE functional. Because only the 1x1x1 unit cell was considered, with four actinide ions, composition resolution was limited to increments of 25%. An equation of state was fitted to each curve to derive predictions for the equilibrium lattice constant and bulk modulus. Those results were compiled into Figure 13 (lattice constant) and Figure 14 (bulk modulus), presenting those predictions alongside the experimentally known values. Again, most MOX systems have not been investigated experimentally; per the results discussed in Section 4.2, all intermediate compositions are assumed to be ideal solid solutions, whose bulk properties vary linearly with composition.

Figure 13 exemplifies the tendency of GGA to underestimate the lattice constant of an actinide-bearing system (a failure of both GGA and LDA without the Hubbard correction), but to do so in a uniform manner. Each system's lattice constant is underestimated by 0.15 Å, and the pure compositions are correctly ordered.
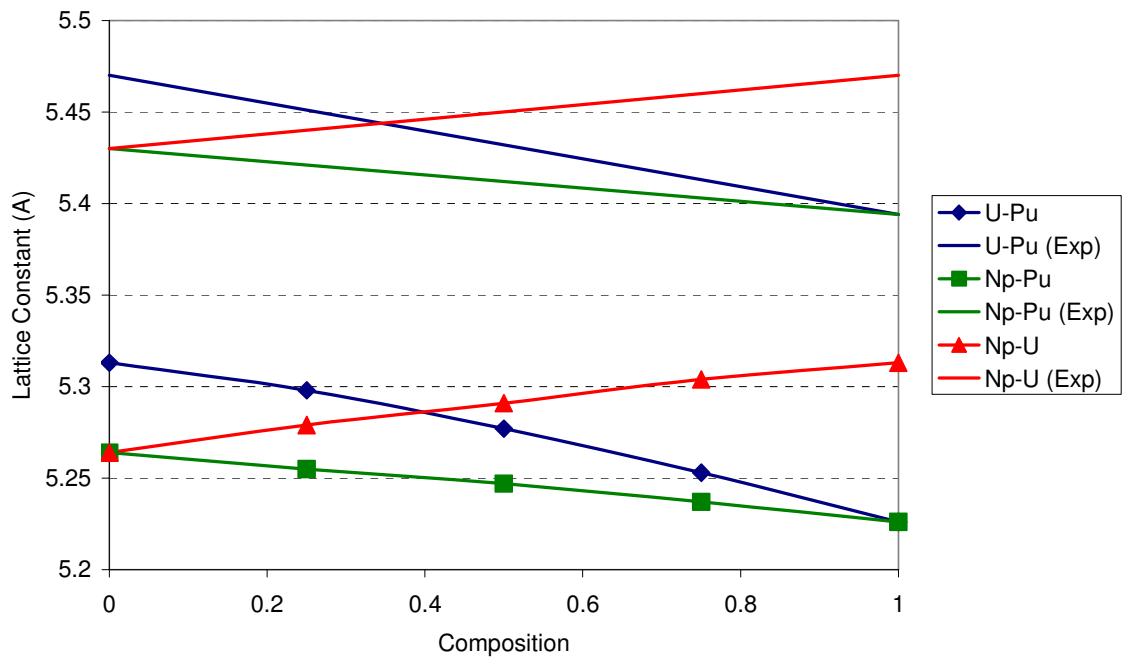
Figure 13: GGA lattice constant predictions of MOX fuels
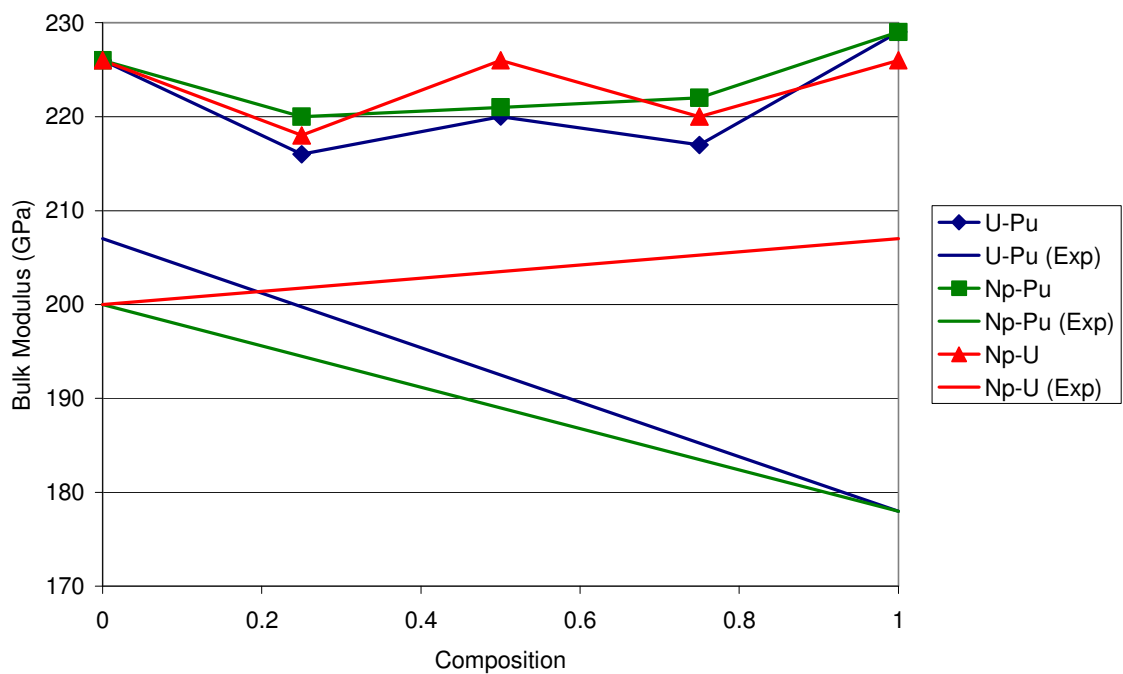
Figure 14: GGA bulk modulus predictions of MOX fuels

In contrast to the well-behaved lattice constant results, Figure 14 displays a rather unordered set of predictions for the bulk moduli. The pure compositions are predicted to have virtually identical values, in contrast to the experimentally known 15% spread between UO_2 and PuO_2. The MOX compositions show no trends, contrary to the suggestion of ideal solid solutions by Figures 12 and 13. The only experimental data available on the topic regards the nonideality of the stoichiometric $(U,Pu)O_2$ solid solution[41], and indicates that ideality resumes at Pu content above 10%, and so no indications of it are likely to be seen with an initial jump from 0 to 25% Pu content.

4.4 Reproducing Metastable States in Pure and Binary Actinide Oxides

4.4.1 Influence of Initial Ion Structure on Metastable States in UO_2

Tests varying only the initial system geometry were run on UO_2 using an LDA+U functional. The simulations plotted in Figure 15 were initialized as an ideal fluorite structure, and the simulations for Figure 16 were initialized with a distortion to the oxygen sublattice. Each oxygen atom was displaced from its idealized (0.25, 0.25, 0.25) fluorite position to the (0.24, 0.24, 0.24) or symmetry-equivalent position.
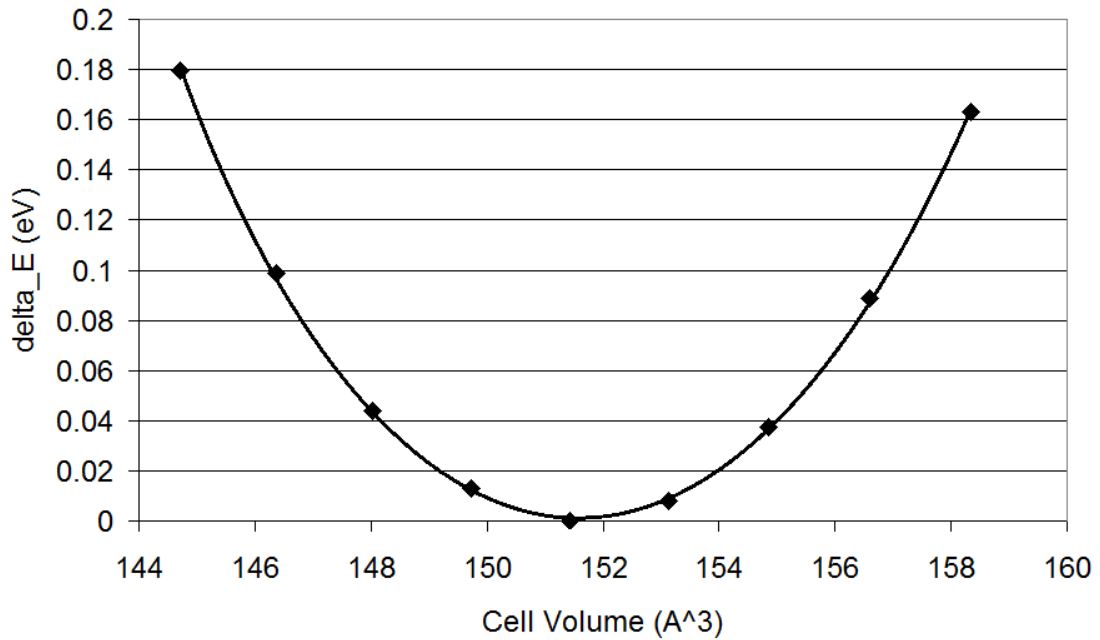
Figure 15: Volume-energy curve for UO_2 +U initialized from ideal fluorite geometry

The ideal initializations all converged to their ground states, while the distorted initial geometries converged to a variety of metastable states, clearly exhibiting the same order of magnitude inferred from Figure 10. Because the known differences for such a curve's ground states are less than 0.1 eV, only the point at 147 $Å^3$ point could potentially be in its ground state. If only two systems were being compared, the presence of metastable states could potentially go unnoticed and pass a standard spot "reality" check. The construction of a volume-energy curve yields the definitive verdict.
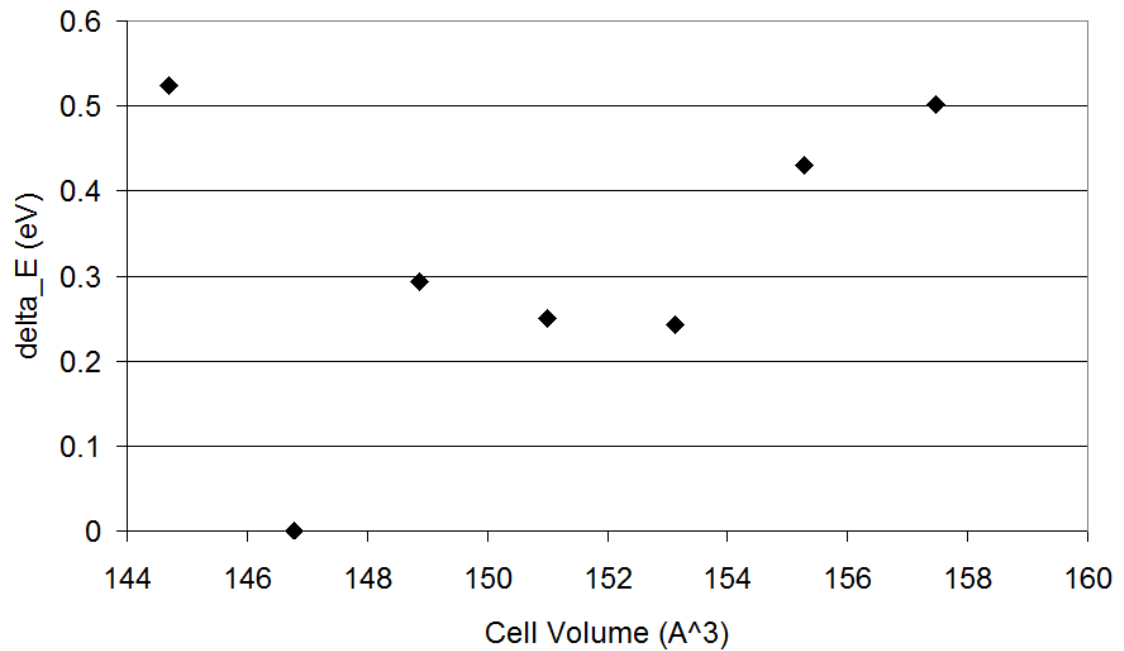
Figure 16: Volume-energy curve for UO_2 +U initialized from distorted geometry

4.4.2 Metastable States in Binary Actinide Oxide Systems

To uncover metastable states in mixed oxide systems, the initialization with a distorted geometry is unnecessary. Figure 17 shows the result of replacing one of the four uranium ions in the ideal fluorite structure of the 1x1x1 unit cell with a plutonium ion, and re-running the systems with sizes centered on the expected equilibrium size.
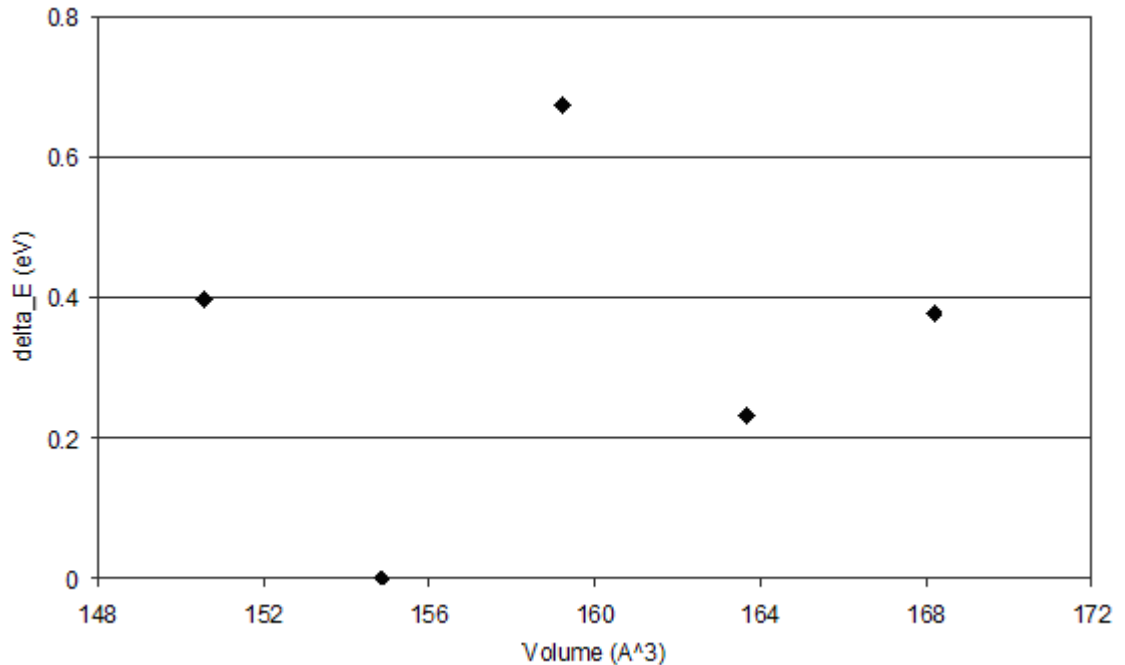
Figure 17: $U_{0.75}Pu_{0.25}O_2$ DFT+U volume-energy curve

The order of magnitude of metastable states is again several tenths of an eV. With their presence established and easily detectable in both pure and mixed oxides, we now move towards methods to avoid them altogether.

4.5 Avoiding Metastable States with Continuation Files

The existing literature methods are fairly time-consuming, requiring a combinatorial search[30] or potentially dozens of consecutive runs for each system size[33]. This work primarily investigated methods involving continuation files, similar to the latter approach by Meredig. As mentioned previously, each simulation output includes not only the converged energy but also the final electronic wavefunctions, charge densities, and ion positions of the simulation. Chosen appropriately after a first iteration of system sizes, these files may initialize a subsequent iteration of systems using sufficiently identical

conditions to converge all systems to the ground state, or potentially to analogous metastable states, which while not ideal, would likely still represent an improvement over non-iterated results. Regardless, the construction of volume-energy curves will provide the insight necessary to classify the results.

4.5.1 Iterated System States

To begin, a series of fixed-size simulations were performed. The volume-energy curve was constructed, and one of the results was chosen (visually) to represent the lowest-lying state. For example, in Figure 16, the 147 Å^3 point would be chosen; in Figure 17, the point at 155 Å^3. The output file for ion positions was copied and scaled in size to represent all other system sizes, and was used, along with its corresponding charge density and wavefunction files, to initialize all system sizes for the second iteration. The process can be repeated multiple times, as shown conceptually in Figure 18, however in practice all compositions either converged after the second iteration or ceased to show progress after five iterations. In every case, the pure compositions converged and the mixed compositions did not.
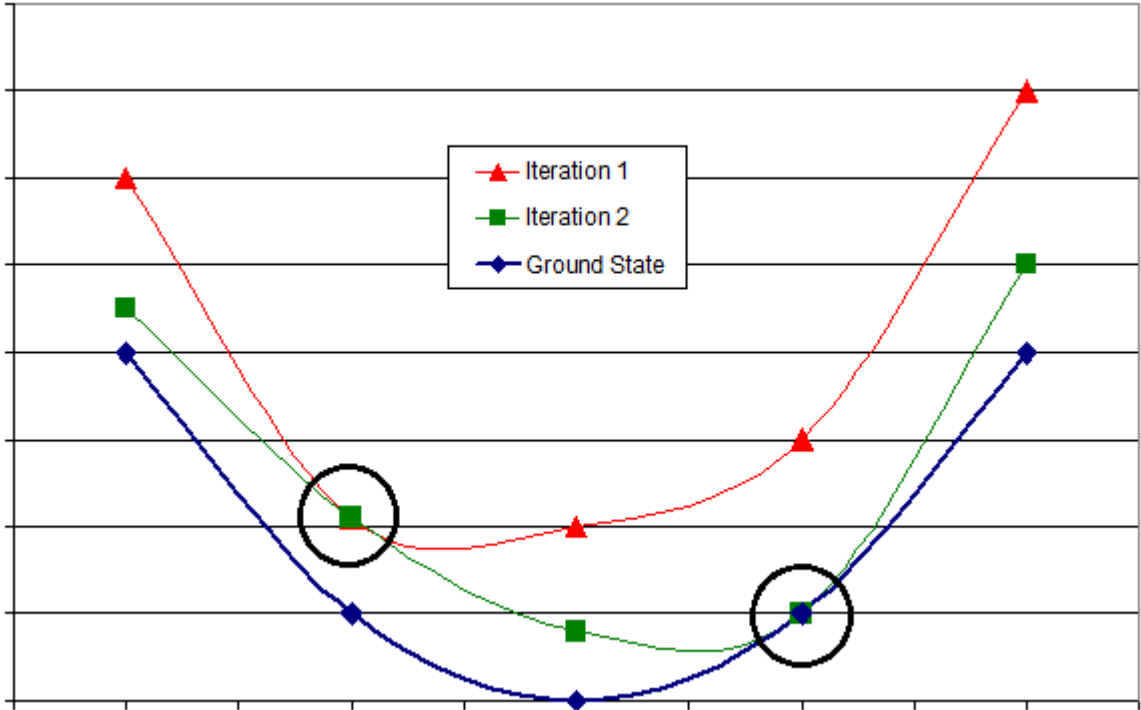
Figure 18: A conceptual sketch of the method of iterated system states

Table 3 lists the theoretical predictions derived for the pure oxides and compares them against known experimental values (Section 2.1) and to another effort from literature.

Table 3: Results for pure actinide oxides using the "iterated system states" approach

	This Work		Experimental Values		Andersson[1]	
	a_0 (Å)	B_0 (GPa)	a_0 (Å)	B_0 (GPa)	a_0 (Å)	B_0 (GPa)
UO_2	5.45	221	5.47	207	5.448	218
PuO_2	5.35	223	5.398	178	5.354	226
NpO_2	5.41	216	5.43	200	5.398	228

The results compare very favorably with both experimental values and existing literature predictions. The high correlation factor between the equation of state and the volume-

energy plots—in excess of 0.99 for all cases—it is apparent that each of the pure actinide oxide systems did indeed reach its ground state.

4.5.2 Cascading System States

It is hypothesized that using the same input continuation files for all system sizes may cause the more sensitive MOX systems to fall into metastable states. A possible solution is to only iterate the continuation files into the most alike systems, i.e. adjacent system sizes.

Beginning with a set of fixed-size systems to simulate, the smallest system was converged. The output file for its converged ion positions was proportionally scaled up to the next-smallest system size, which, along with its output wavefunction and charge density files, was used to initialize that system. The results of this second-smallest system were scaled up and used as initial conditions for the third-smallest system, effectively being "cascaded" from one system to the next, repeated up to the largest system size.
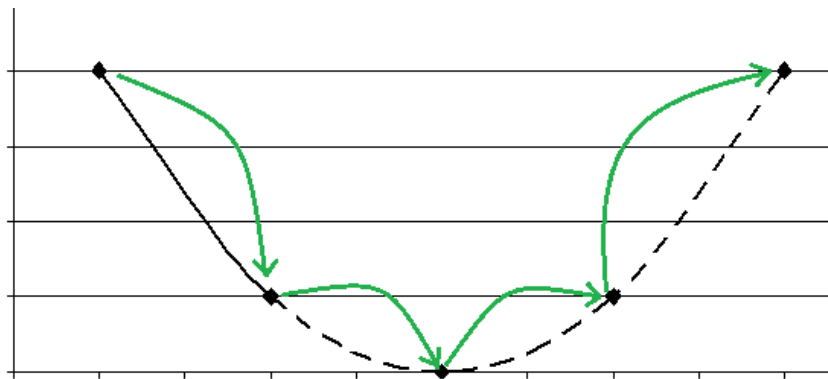
Figure 19: The concept of cascading system states

In the event that metastable noise is present after the first pass, the option exists to then perform a reverse pass, starting with the largest system size and working back down to the smallest. An alternate scheme is to begin the entire process with an intermediate-sized system and cascade results towards both extremes independently. Either process should be terminated if either the volume-energy curve becomes smooth, or if two consecutive iterations fail to yield a lower energy for any system size.
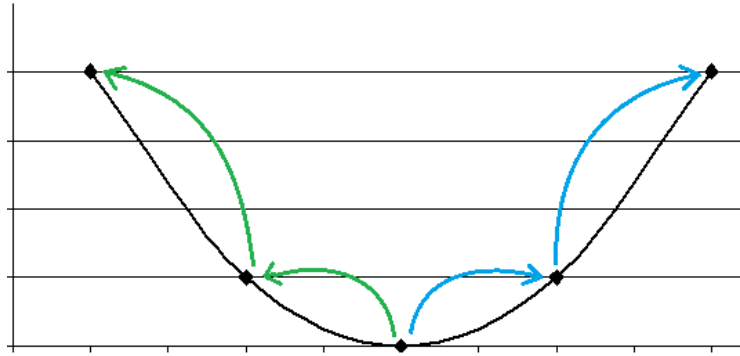
Figure 20: An alternate "cascading system states" scheme

Both schemes were attempted for all systems; the pure AO_2 results for the scheme with the stronger fit (measured by the regression's R^2 value) are shown in Table 4.

Table 4: Results for pure actinide oxides using the "cascading system states" approach

	This Work			Experimental Values	
	a_0 (Å)	B_0 (GPa)	R^2 value	a_0 (Å)	B_0 (GPa)
UO_2	5.46	110	0.71	5.47	207
PuO_2	5.35	336	0.94	5.398	178
NpO_2	5.51	704	0.41	5.43	200

Neither cascade scheme yielded progress for MOX systems, and, further, failed to achieve success with the more well-behaved pure compositions. The pure compositions showed too little improvement over naive +U results to recommend the method in any serious capacity. Neptunia failed to show any improvement, and although urania and plutonia improved sufficiently to adequately predict lattice parameters, the best-fit equations of state predicted bulk moduli with errors exceeding 50%.

CHAPTER 5: CONCLUSIONS

Metastable states are a genuine challenge when probing nuclear oxide fuels via DFT calculations. Existing methods have been spot-checked in multiple cases, but a volume-energy curve could provide a more rigorous test. With its small tolerance for metastable noise and abundance of similar but nonidentical systems whose ground states are very close in energy, it is well suited to do so; the small energy differences between adjacent systems are known to follow a particular trend, and the presence of metastable states introduces a pronounced disruption.

There remains much work to be done in the DFT investigation of actinide oxides, in particular the MOX compositions, but it should prove fruitful. There already exist two well-established literature methods for overcoming metastable states in pure urania, and the method of iterated system states outlined in Subsection 4.5.1 looks to be a promising addition, although its approach may restrict it to the investigation energy differences between systems with a high degree of geometric similarity. Where it is valid, systems appear to converge to their ground states with considerably less computational cost than would be required with the combinatorial approach suggested by Dorado[30] or the gradual parameterization outlined by Meredig[33].

MOX compositions remain especially resilient to all methods attempted here, and the combinatorial explosion which would emerge by applying the Dorado approach quickly makes it unrealistic. The Meredig method, although slightly more organic, now would be

tasked with the simultaneous ramping of multiple species' Hubbard parameters. With the

quantitative behavior of the energy surface still far beyond comprehension, a

combinatorial approach may be required here as well for MOX systems, to determine

whether species' +U values should be ramped simultaneously, in sequence, or in parallel.

Clearly, more effective methods are required in this realm.

REFERENCES

[1] Andersson et al. "Cooperativity among defect sites in $AO_{2\pm x}$." *Physical Review B* **79**, 024110 (2009).

[2] Bairiot et al (2003). *Status and Advances in MOX Fuel Technology* (Technical Reports Series No. 415). Vienna: International Atomic Energy Agency.

[3] Stan et al. "Models and simulations of nuclear fuel material properties." *Journal of Alloys and Compounds* **444-445**, 415-423 (2007).

[4] Yamashita et al. "Thermal expansion of neptunium-uranium mixed oxides." *Journal of Nuclear Materials* **247**, 90-93 (1997).

[5] Idiri et al. "Behavior of Actinide Dioxides Under Pressure." *Physical Review B* **70**, 014113 (2004).

[6] Haschke, Allen and Morales. "Reaction of Plutonium Dioxide with Water: Formation and Properties of PuO_{2+x}." *Science* **287**, 285-287 (2000).

[7] Santini et al. "Multipolar interactions in f-electron systems: The paradigm of actinide dioxides." *Reviews of Modern Physics* **81**, 807-863 (2009).

[8] Gryaznov, Heifets and Kotomin. "Ab initio DFT+U study of He atom incorporation into UO_2 crystals." *Physical Chemistry Chemical Physics* **11**, 7241 (2009).

[9] Payne et al. "Iterative minimization techniques for *ab initio* total-energy calculations: molecular dynamics and conjugate gradients." *Reviews of Modern Physics* **64**, 1045-1097 (1992).

[10] Hohenberg and Kohn. "Inhomogeneous Electron Gas." *Physical Review* **136**, B864 (1964).

[11] Kohn and Sham. "Self-Consistent Equations Including Exchange and Correlation Effects." *Physical Review* **140**, A1133 (1965).

[12] Sherrill, David. "The Correlation Energy." Retrieved May 2011, from http://vergil.chemistry.gatech.edu/notes/ci/node6.html

[13] Askerov, Bahram and Figarova, Sophia. "Thermodynamics, Gibbs Method and Statistical Physics of Electron Gases." Springer, 2010.

[14] Slater, John Clarke. "Quantum Theory of Molecules and Solids: The self consistent field for molecules and solids (Volume IV)." McGraw-Hill, New York, 1974.

[15] Gunnarsson and Lundqvist. "Exchange and correlation in atoms, molecules, and solids by the spin-density-functional formalism." *Physical Review B* **13**, 4274-4298 (1976).

[16] Harrison, N.M. "An Introduction to Density Functional Theory." Department of Chemistry, Imperial College of Science Technology and Medicine. Retrieved January 2012, from http://www.ch.ic.ac.uk/harrison/Teaching/DFT_NATO.pdf

[17] Perdew, Burke, and Ernzerhof. "Generalized Gradient Approximation Made Simple." *Physical Review Letters* **77**, 3865 (1996); errata found at *Physical Review Letters* **78**, 1396 (1997).

[18] Becke. "Density-functional exchange-energy approximation with correct asymptotic behavior." *Physical Review A* **38**, 3098 (1988).

[19] Perdew et al. "Accurate Density Functional with Correct Formal Properties: A Step Beyond the Generalized Gradient Approximation." *Physical Review Letters* **82**, 2544 (1999); errata found at *Physical Review Letters* **82**, 5179 (1999).

[20] Boettger and Ray. "All-electron LCGTO calculations for uranium dioxide." *International Journal of Quantum Chemistry* **80**, 824-830 (2000).

[21] Boettger and Ray. "Fully relativistic density functional calculations on hydroxylated actinide oxide surfaces." *International Journal of Quantum Chemistry* **90**, 1470-1477 (2002).

[22] Ashcroft and Mermin. "Solid State Physics." Brooks Cole, 1976.

[23] Monkhorst and Pack. "Special points for Brillouin-zone integrations." *Physical Review B* **13**, 5188 (1976).

[24] Dudarev et al. "Electronic Structure and Elastic Properties of Strongly Correlated Metal Oxides from First Principles: LSDA+U, SIC-LSDA and EELS Study of UO_2 and NiO." *Solid State Physics* **166**, 429 (1998).

[25] Dudarev et al. "Effect of Mott-Hubbard correlations on the electronic structure and structural stability of uranium dioxide." *Philosophical Magazine Part B* **75**, 613-628 (1997).

[26] Crocombette. "Ab initio energetics of some fission products (Kr, I, Cs, Sr and He) in uranium dioxide." *Journal of Nuclear Materials* **305**, 29-36 (2002).

[27] Freyss, Petit, and Crocombette. "Point defects in uranium dioxide: Ab initio pseudopotential approach in the generalized gradient approximation." *Journal of Nuclear Materials* **347**, 44 (2005).

[28] Geng, Chen, Kaneta, and Kinoshita. "Structural behavior of uranium dioxide under pressure by LSDA+U calculations." *Physical Review B* **75**, 054111 (2007).

[29] Gupta, Brillant, and Pasturel. "Correlation effects and energetics of point defects in uranium dioxide: a first principles investigation." *Philosophical Magazine* **87**, 2561 (2007).

[30] Dorado et al. "DFT+U calculations of the ground state and metastable states of uranium dioxide." *Physical Review B* **79**, 235125 (2009).

[31] Meek, Thomas. "Semiconductive Properties of Uranium Oxides." Materials Science Engineering Department, University of Tennessee. For the Waste Management 2001 Symposium.

[32] Anisimov, Zaanen, and Andersen. "Band theory and Mott insulators: Hubbard *U* instead of Stoner *I*." *Physical Review B* **44** 943-954 (1991).

[33] Meredig et al. "Method for locating low-energy solutions within DFT+U." *Physical Review B* **82**, 195128 (2010).

[34] Murnaghan, F. "The Compressibility of Media under Extreme Pressures." *Proceedings of the National Academy of Sciences of the United States of America* **30**, 244-247 (1944).

[35] Birch, F. "Finite Elastic Strain of Cubic Crystals." *Physical Review* **71**, 809-824 (1947).

[36] Kresse and Furthmuller. "Efficiency of ab-initio total energy calculations for metals and semiconductors using a plane-wave basis set." *Computational Materials Science* **6**, 15-50 (1996).

[37] Kresse and Furthmuller. "Efficient iterative schemes for ab-initio total-energy calculations using a plane-wave basis set." *Physical Review B* **54**, 11169-11186 (1996).

[38] Kotani, Akio and Yamazaki, Takao. "Systematic Analysis of Core Photoemission Spectra for Actinide Di-Oxides and Rare-Earth Sesqui-Oxides." *Progress of Theoretical Physics* **Supplement No. 108**, 117-131 (1992).

[39] Dudarev et al. "Electron-loss energy spectra and the structural stability of nickel oxide: An LSDA+U study." *Physical Review B* **57**, 1505-1509 (1998).

[40] Lyon and Baily. "The solid-liquid phase diagram for the UO_2-PuO_2 system." *Journal of Nuclear Materials* **22**, 332-339 (1967).

[41] Beauvy, Michel. "Nonideality of the solid solution in $(U,Pu)O_2$ nuclear fuels." *Journal of Nuclear Materials* **188**, 232-238 (1992).